DOI: 10.1002/ange.201306306

PET/MRI Agents

Chelator-Free Synthesis of a Dual-Modality PET/MRI Agent**

*Feng Chen, Paul A. Ellison, Christina M. Lewis, Hao Hong, Yin Zhang, Sixiang Shi, Reinier Hernandez, M. Elizabeth Meyerand, Todd E. Barnhart, and Weibo Cai**

Most of the radiometals with physical properties suitable for imaging and/or therapy applications (including ^{64}Cu, ^{89}Zr, ^{99m}Tc, ^{111}In, ^{177}Lu, and ^{90}Y) require the coordination of certain chelators to form stable complexes.[1] Because of the uniqueness of each radionuclide, knowing the particular coordination chemistry and selecting the best chelator for sufficient in vivo stability are vital, but highly challenging tasks. Therefore, the development of a stable radiopharmaceutical that contains both diagnostic and therapeutic radioisotopes and is labeled by a simple but effective chelator-free strategy is highly desirable.

The combination of positron emission tomography (PET) and magnetic resonance imaging (MRI) has attracted tremendous interest over the last decade, and PET/MRI scanners have become commercially available.[2] The future of PET/MRI scanning will greatly benefit from the use of dual-modality PET/MRI probes. Many dual-modality PET/MRI agents have been reported; these are typically synthesized by the radiolabeling of magnetic nanoparticles.[3]

Arsenic (As) has four positron-emitting ($^{70/71/72/74}$As) and three electron-emitting ($^{74/76/77}$As) radioisotopes with half-lives ranging from 52.6 min to 17.8 days (Supporting Information, Table S1), which could be useful for both PET and internal radiotherapy applications.[1] However, arsenic isotopes have been scarcely used because of limited availability and difficulties related to isotope production and separation and the purity of the radionuclides.[4] Furthermore, few techniques are currently available for the incorporation of these radionuclides into biologically relevant targeting vectors. To the best of our knowledge, the labeling of antibodies and polymers through covalent interactions of radioactive arsenite, namely *As^{III}, with sulfhydryl groups is the only reported method,[5] whereas techniques for the labeling of radioactive arsenate, namely *As^{V}, are still unavailable.

Fortunately, the incorporation of both As^{III} and As^{V} into magnetite or superparamagnetic iron oxide nanoparticle (SPION) structures has been observed for a long time, and it is still used for groundwater decontamination processes.[6] Furthermore, the underlying chemical mechanism of this highly specific and efficient arsenic trapping by magnetite was also elucidated recently.[7] The high affinity of arsenic for the magnetite surface has been suggested to be related to the formation of highly stable As complexes, where As$^{III}O_3$ trigonal pyramids or As$^{V}O_4$ tetrahedra occupy vacant FeO_4 tetrahedral sites on the octahedrally terminated {111} surface of the magnetite nanoparticles.[7]

Inspired by these results, we have now developed a simple, but highly efficient strategy for the synthesis of radioarsenic-labeled SPIONs (*As-SPIONs; * = 71, 72, 74, 76) without the use of any chelators. We hypothesized that by mixing water-soluble SPIONs with *As^{III} or *As^{V} species, the novel dual-modality PET/MRI agent *As-SPION could be easily formed because of the strong and specific affinity of *As for the SPION surface (Figure 1a).

The transmission electron microscopy (TEM) image of oleic acid (OA)-capped SPIONs with a diameter of ca. 10 nm and irregular morphologies, which were synthesized following a well-established thermal decomposition method, is shown in Figure 1b.[8] These SPIONs were coated with a layer of OA surfactant; the resulting particles were only well-dispersed in nonpolar organic solvents (e.g., cyclohexane) and exhibited superparamagnetism at room temperature (Figure 1b, inset). The X-ray diffraction pattern of as-synthesized SPION matches well with the standard Fe_3O_4 reflection (JCPDS No. 89-0691; Figure S1). A well-established ligand-exchange process was used to replace the original OA ligands with poly(acrylic acid) (PAA),[9] and efficiently transferred SPION@OA from the organic phase to the aqueous phase (Figure 1c, inset), which resulted in PAA-modified SPIONs (SPION@PAA). A TEM image (Figure 1c) confirmed that there is no obvious change of the SPIONs in either particle size or morphology after ligand exchange. Dynamic light scattering (DLS) analysis of SPION@PAA in phosphate-buffered saline (PBS; pH 7.4) solution indicated a diameter of 23.1 nm (which includes the surface coating and the hydration layer), which is larger than the core size observed by TEM (ca. 10 nm). As-synthesized SPION@PAA was found to be highly stable in many different biological solutions, such as PBS, saline, and fetal bovine serum, with no visible aggregation after more than six months (Figure S2).

[*] Dr. F. Chen,[+] Dr. H. Hong, Prof. W. Cai
Department of Radiology, University of Wisconsin-Madison
1111 Highland Avenue, Madison, WI, 53705 (USA)
E-mail: WCai@uwhealth.org
Homepage: http://mi.wisc.edu
Dr. P. A. Ellison,[+] C. M. Lewis, Dr. Y. Zhang, R. Hernandez, Prof. M. E. Meyerand, Dr. T. E. Barnhart, Prof. W. Cai
Department of Medical Physics
University of Wisconsin-Madison, WI (USA)
S. Shi, Prof. W. Cai
Materials Science Program
University of Wisconsin-Madison, WI (USA)
[+] F.C. and P.A.E. contributed equally to this work.

[**] This work is supported in part by the University of Wisconsin-Madison, the National Institutes of Health (NIBIB/NCI 1R01CA169365, T32CA009206, and T32GM08349), the Department of Defense (W81XWH-11-1-0644), and the American Cancer Society (125246-RSG-13-099-01-CCE). The authors thank Prof. R. J. Nickles and Prof. O. T. DeJesus for helpful discussions related to the production and isolation of radioarsenic.

Supporting information for this article is available on the WWW under http://dx.doi.org/10.1002/anie.201306306.

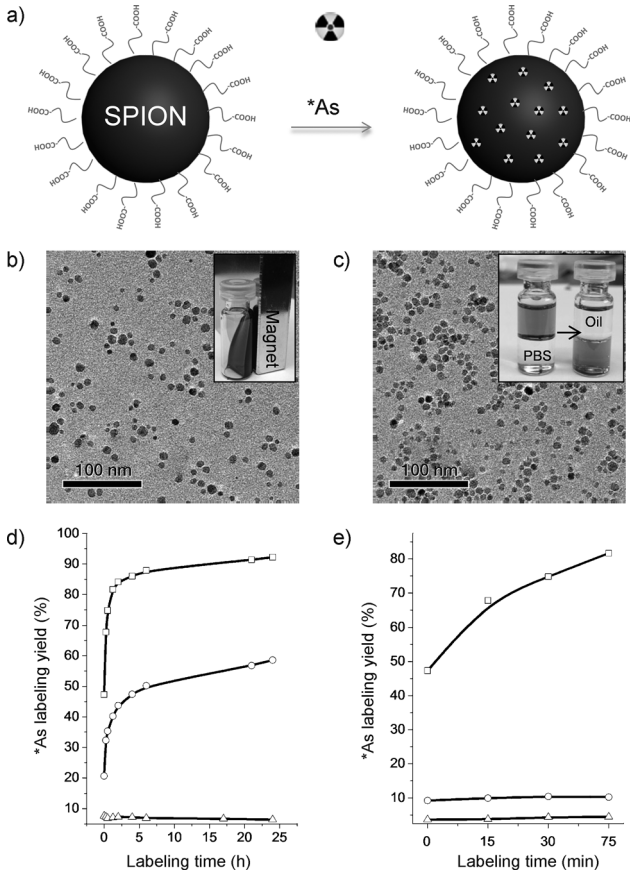

Figure 1. a) Chelator-free synthesis of *As-SPIONs. b) TEM image of SPION@OA. Inset: photograph showing the ferrofluidic behavior of SPION@OA in cyclohexane at room temperature. c) TEM image of SPION@PAA. Inset: transfer of SPION@OA from the oil phase (cyclohexane) to the aqueous phase (PBS, pH 7.4) by exchanging the OA ligand for PAA. d) Time-dependent *As labeling yield of SPION@PAA (□) and partial adsorption blocking by competitive sodium citrate ions (○). For the negative control group (△), only water (pH 7–8, 1 mM of sodium hydroxide) and radioarsenic (ca. 6 MBq) were used. e) Influence of the nanoparticle surface on the *As labeling yield for SPION@PAA (□), CuS (○), and SPION@dSiO_2 (△).

Radioarsenic was produced by irradiating natural germanium oxide targets with protons using the University of Wisconsin GE PETtrace Cyclotron. Irradiated targets were processed in a multistep chemical-isolation procedure adapted from the literature,[5c,10] which involves dissolution, precipitation, filtration, evaporation, anion exchange chromatography, reduction, and solvent extraction. This four-hour procedure gave a non-decay-corrected radioarsenic yield of $49 \pm 12\%$ ($n = 13$), and resulted in a mixture of $*As^{III}$ and $*As^{V}$ in a small volume of aqueous solution (pH 4.5) with no detectable radiocontaminants.

The oxidation state of radioarsenic at the end of the separation procedure was initially $*As^{III}$; the radioarsenic was present as $*As(OH)_3$, which was observed to rapidly autoxidize to $*As^{V}$, thus forming H_3*AsO_4. The rate of this autoxidation varied widely over the conducted experiments. As a result, the following experiments for the *As labeling of SPIONs were conducted with a mixture of $*As^{III}$ as $*As(OH)_3$ and $*As^{V}$ as $[H_2*AsO_4]^{1-}$ and $[H*AsO_4]^{2-}$ in solution, with the $*As^{III}/*As^{V}$ ratio ranging from < 0.1 to approximately 0.8. The oxidation state of the radioarsenic could be monitored through separation and nanoparticle-labeling procedures using thin layer chromatography (TLC) that was visualized by autoradiography.

The pH- and oxidation-state-dependent sorption behaviors of arsenic to magnetite have already been well-documented.[6d] Considering the co-existence of $*As^{III}$ and $*As^{V}$ after the generation of radioarsenic, we fixed the pH to 7–8 for the optimization of the *As labeling yield. Radiolabeling yields were calculated by spotting analyte on styrene-backed SiO_2 (250 μm) TLC plates, which were developed with a sodium tartrate/methanol (3:1; 0.01M) solution as the mobile phase. The distribution of radioarsenic was visualized by exposing a Packard multisensitive phosphor screen to the developed, dried, and tape-covered plates, followed by processing with a PerkinElmer Cyclone Plus Storage Phosphor System. *As-SPION nanoparticles ($R_F = 0$) could be easily distinguished from free $*As^{III}$ ($R_F \approx 0.8$) and $*As^{V}$ ($R_F \approx 0.95$) using this analytical procedure (Figure S3).

Immediately after the mixing of *As with water-soluble SPION@PAA in NaOH (1 mM) at pH 7–8, 47.3% of *As was strongly adsorbed to the SPION surface (Figure 1d,e). The *As labeling yield exhibited a sharp increase to 84.2% within 2 h of incubation (specific radioactivity ca. 3.0 MBq μmol^{-1} of Fe), and slowly reached the maximum labeling yield of 92.2% after 24 h (Figure 1d and Figure S4a). Negative-control experiments (Figure 1d and Figure S4c) without SPION were performed to confirm the successful labeling of SPION with *As.

Competitive adsorption between As and other ions (e.g., phosphate and citrate) to iron oxides has been reported.[11] For example, adsorption of As^{III} and As^{V} on hydrated iron oxide could be suppressed in the presence of phosphate.[11b] To confirm the specific adsorption of *As to SPION, a solvent with competitive ions originating from sodium citrate (17 mM, pH 7–8) was used to inhibit the adsorption of *As to SPION. An approximately two-fold reduction of the *As labeling yield was observed after two hours of incubation (43.7% vs. 84.2%) of *As with SPION@PAA and sodium citrate (Figure 1d; see also Figure S4b). No significant changes in the *As labeling yield were observed after further increasing the concentration of sodium citrate to 340 mM (Figure S5a). The dependence of the *As labeling yield on the iron concentration was also demonstrated, as a higher SPION concentration led to an increase in the *As labeling yield as expected (Figure S5b).

We hypothesize that the coating of SPIONs with a dense silica (dSiO_2) shell or incubating *As with non-magnetite nanoparticles could prevent the adsorption of *As, as they are not expected to form stable $*As^{III}$ or $*As^{V}$ complexes.[7] To further demonstrate the high specificity of the SPION labeling with *As, two control studies were performed. Incubation of the same amount of *As with citrate-capped copper sulfide (CuS) nanoparticles or SPION@dSiO_2 led to no obvious *As labeling (Figure 1e and Figure S6), clearly indicating the high labeling efficiency and specificity of *As to SPION. Taken together, our systematic investigation illustrated the successful labeling of SPION with *As, which is

a fast, iron-concentration-dependent, and highly specific process.

To examine the capability of *As-SPIONs for dual-modality PET/MRI, phantom studies were first performed. PET images of *As-SPIONs at various levels of radioactivity (0–1.50 MBq) and Fe concentrations (0–15.5 mM) are shown in Figure 2a and 2b. As no radioactive materials (e.g., *As-SPION) are allowed in our 4.7 T microMRI scanning room, SPIONs with the same Fe concentrations as in Figure 2b were used to demonstrate the enhanced T_2* MR contrast. A decrease of the T_2 relaxation time (from 484.4 to 5.4 ms) was observed with an increase in Fe concentration (from 0 to 1.94 mM), which is consistent with the corresponding T_2* weighted MR images (Figure 2c). The relaxation time T_2 was too short to be measured at Fe concentrations equal to or exceeding 3.88 mM, because of the absence of a measurable signal (indicated by dashed circles). The T_2 relaxivity (r_2) of SPION@PAA was found to be 93.8 $mM^{-1}s^{-1}$ in the 4.7 T microMRI scanner (Figure S7).

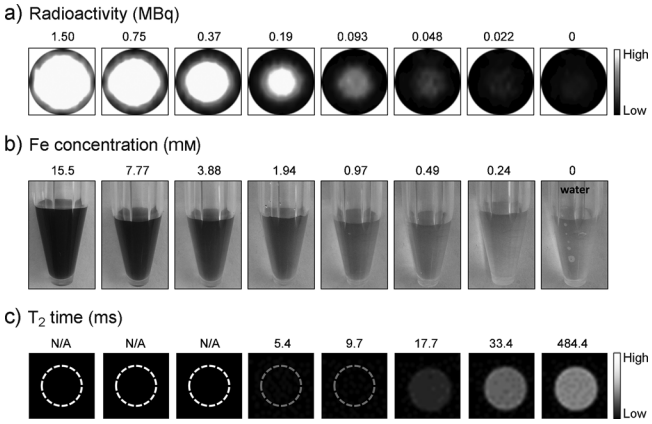

Figure 2. a) PET imaging of *As-SPION (in a 0.25 mM HEPES buffer) at various radioactivity levels (0–1.50 MBq). b,c) Digital photographs (b) and corresponding T_2*-weighted MR images of SPION@PAA (c) at various Fe concentrations (0–15.5 mM). The T_2 relaxation time was too short to be measured at Fe concentrations $\geq$3.88 mM (dashed circles).

To demonstrate the feasibility of *As-SPIONs for dual-modality PET/MRI imaging and to investigate their biodistribution in vivo, an *As-SPION solution (200 μL, ca. 5.5 MBq) was intravenously injected into normal BALB/c mice. Strong uptake of *As-SPIONs by the liver (32.5 ± 0.7, 25.7 ± 1.6, and 16.1 ± 2.5 %ID/g at 0.5, 2.5, and 15 h post-injection (p.i.), respectively; $n = 2$; %ID/g = percentage of the injected dose per gram) and the bladder (18.5 ± 3.2, 58.3 ± 5.6, and 5.3 ± 4.9 %ID/g at 0.5, 2.5, and 15 h p.i., respectively) was observed (Figure 3b). As the DLS diameter of *As-SPION is significantly larger than the renal clearance threshold (ca. 5.5 nm),[12] the radioactivity signal of the bladder is likely due to the desorption of *As from SPION under biological conditions.

We further demonstrated that this desorption of *As could be significantly reduced by coating *As-SPIONs with a layer of poly(ethylene glycol) (PEG). Strong liver uptake of

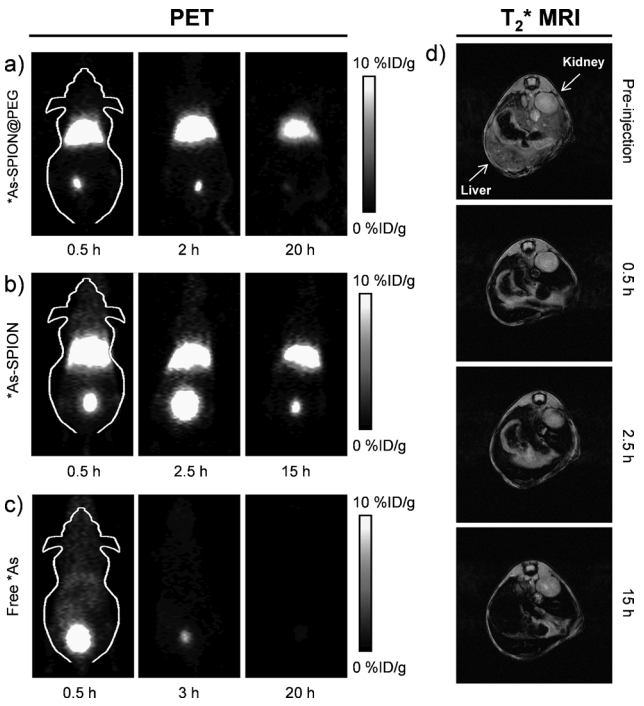

Figure 3. a–c) Serial in vivo PET images of PEGylated *As-SPIONs (a), non-PEGylated *As-SPIONs (b), and free *As (c) at different time points after intravenous injection into mice. d) In vivo T_2*-weighted MR images of mice before and after intravenous injection of SPION@PAA (in PBS). Transaxial images are presented to show the liver uptake of SPION@PAA.

*As-SPION@PEG was observed (25.0 ± 2.7, 24.8 ± 3.2, 11.0 ± 1.4 %ID/g at 0.5, 2, and 20 h p.i., respectively; $n = 4$), with a significantly decreased bladder signal (12.0 ± 1.3, 11.7 ± 3.2, 3.9 ± 2.2 %ID/g at 0.5, 2, and 20 h p.i., respectively; $n = 4$) after intravenous injection of *As-SPION@PEG into mice (Figure 3a). The enhanced stability of *As-SPION@PEG was also confirmed by incubation in complete mouse serum at 37 °C for 24 h (Figure S8). Nevertheless, efforts towards further optimizing the stability of *As-SPIONs in vivo are necessary.

In comparison with the biodistribution patterns of free *As (Figure 3c), which show fast renal clearance and nearly no liver uptake of *As, the strong radioactivity signal from the liver (Figure 3a,b) indeed originated from *As-SPION@PEG (or *As-SPIONs), but not from free *As. The liver uptake of *As-SPIONs was further confirmed by in vivo MR imaging, which clearly showed darkening of the liver and no detectable signal change for the kidney (or bladder) after intravenous injection of SPION@PAA (Figure 3d). The biodistribution of *As-SPION@PEG was further investigated at 20 h p.i., after euthanizing the mice after the final PET scan and by measuring the tissue radioactivity with a γ-counter (Figure S9). Dominant uptake of *As-SPION@PEG by both liver and spleen was observed, which validated that the serial PET imaging (Figure 3a) truly reflected the distribution pattern of *As-SPION@PEG in mice. Similar uptakes of the other PET/MRI contrast agents (e.g., ^{64}Cu-labeled SPION) by liver and spleen have previously been reported,

and are commonly observed for intravenously injected nanoparticles.[3b,13]

The lymphatic system is an important first line of defense against infection, and it is also a common route for cancer metastasis.[14] Therefore, sentinel-lymph-node mapping is of critical importance in clinical cancer patient treatment.[15] We demonstrated that *As-SPION@PEG could also be used as a dual-modality PET/MRI probe for lymph-node mapping. Upon subcutaneous injection of an *As-SPION@PEG solution (40 μL, ca. 3 MBq) into the right footpad of normal BALB/c mice, serial PET scans were performed. Accumulation of *As-SPION@PEG in the popliteal lymph node could clearly be seen at 2.5 and 15 h p.i. (Figure 4a), with uptakes of *As-SPION@PEG of 12.5 and 13.2 %ID/g, respectively (Figure 4b). The accumulation of SPION@PAA

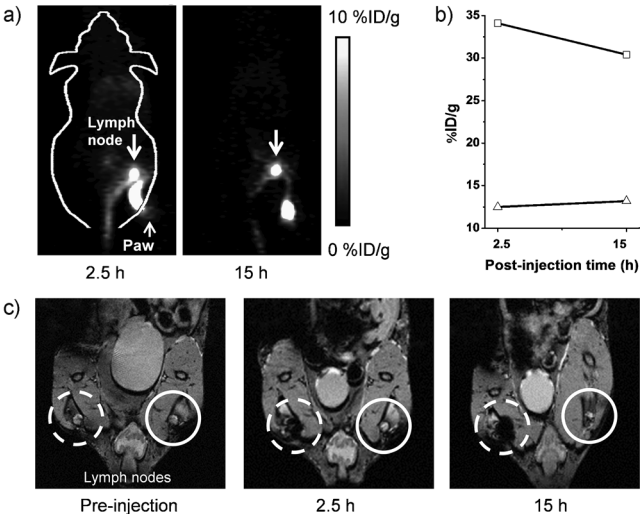

Figure 4. a) In vivo lymph-node imaging with PET after subcutaneous injection of *As-SPION@PEG into the right footpad of the mouse. b) Quantification of the *As-SPION@PEG uptake by the lymph node (△) and the mouse paw (□). c) In vivo lymph-node mapping with MRI, before and after injection of SPION@PAA into the left footpad of the mouse. Obvious darkening of the lymph node could be seen (dashed circle), whereas no contrast enhancement was observed for the contralateral lymph node (solid circle).

in one of the lymph nodes (dashed circle in Figure 4c) could also be clearly visualized by MRI, which showed gradual darkening of the lymph node after injection of SPION@PAA (40 μL, 7.77 mM of Fe) into the footpad of mice. As an internal control, the contralateral lymph node (solid circle in Figure 4c) showed no contrast enhancement.

Although dual-modality PET/MRI imaging could only be achieved separately in our current work because of the lack of an integrated microPET/microMRI scanner, this work serves as an important proof of concept to establish *As-SPIONs as a promising candidate for simultaneous PET/MRI. With further development of scanners that integrate whole-body MRI with a simultaneous acquisition of PET, such as the Siemens Biograph mMR system, imaging agents like *As-SPION will be required to take advantage of the high sensitivity of PET and the exquisite soft-tissue contrast of MRI for future cancer patient treatment. As the labeling of radioarsenic is not limited to positron-emitting *As, other radioarsenic isotopes with therapeutic capability (e.g., $^{76/77}$As) could also be readily used for the integration of PET/MRI imaging with internal radiotherapy. With the presence of carboxyl groups at the surface of *As-SPIONs, further conjugation of specific targeting ligands, such as proteins, antibodies, or peptides,[16] could be readily achieved, which would make this class of agents even more powerful for future cancer-targeted PET/MRI and simultaneous radiotherapy, as well as many other clinical scenarios.

In conclusion, we have developed a novel dual-modality PET/MRI agent, *As-SPIONs, by mixing irregularly-shaped SPIONs with radioarsenic. In comparison with the majority of PET/MRI agents reported to date,[3,17] our method does not require the use of any chelators and is applicable for labeling radioarsenic in both stable oxidation states. Upon optimization, *As labeling of SPION was demonstrated to be fast, iron-concentration-dependent, and highly specific. The biodistribution pattern and the feasibility of our new PET/MRI agent for in vivo dual-modality imaging and lymph-node mapping have also been investigated.

Received: July 19, 2013
Published online: October 24, 2013

Keywords: arsenic · cancer · magnetic resonance imaging · positron emission tomography · radiochemistry

[1] C. S. Cutler, H. M. Hennkens, N. Sisay, S. Huclier-Markai, S. S. Jurisson, *Chem. Rev.* **2013**, *113*, 858–883.
[2] S. Balyasnikova, J. Lofgren, R. de Nijs, Y. Zamogilnaya, L. Hojgaard, B. M. Fischer, *Am. J. Nucl. Med. Mol. Imaging* **2012**, *2*, 458–474.
[3] a) J. S. Choi, J. C. Park, H. Nah, S. Woo, J. Oh, K. M. Kim, G. J. Cheon, Y. Chang, J. Yoo, J. Cheon, *Angew. Chem.* **2008**, *120*, 6355–6358; *Angew. Chem. Int. Ed.* **2008**, *47*, 6259–6262; b) H. Y. Lee, Z. Li, K. Chen, A. R. Hsu, C. Xu, J. Xie, S. Sun, X. Chen, *J. Nucl. Med.* **2008**, *49*, 1371–1379.
[4] M. Jennewein, S. M. Qaim, A. Hermanne, M. Jahn, E. Tsyganov, N. Slavine, S. Seliounine, P. A. Antich, P. V. Kulkarni, P. E. Thorpe, R. P. Mason, F. Rosch, *Appl. Radiat. Isot.* **2005**, *63*, 343–351.
[5] a) M. Jennewein, A. Hermanne, R. P. Mason, P. E. Thorpe, F. Rösch, *Nucl. Instrum. Methods Phys. Res.* **2006**, *569*, 512–517; b) M. Jennewein, M. A. Lewis, D. Zhao, E. Tsyganov, N. Slavine, J. He, L. Watkins, V. D. Kodibagkar, S. O'Kelly, P. Kulkarni, P. P. Antich, A. Hermanne, F. Rosch, R. P. Mason, P. E. Thorpe, *Clin. Cancer Res.* **2008**, *14*, 1377–1385; c) M. Jahn, V. Radchenko, D. Filosofov, H. Hauser, M. Eisenhut, F. Rosch, M. Jennewein, *Radiochim. Acta* **2010**, *98*, 807–812; d) M. M. Herth, M. Barz, M. Jahn, R. Zentel, F. Rosch, *Bioorg. Med. Chem. Lett.* **2010**, *20*, 5454–5458.
[6] a) C. T. Yavuz, J. T. Mayo, W. W. Yu, A. Prakash, J. C. Falkner, S. Yean, L. Cong, H. J. Shipley, A. Kan, M. Tomson, D. Natelson, V. L. Colvin, *Science* **2006**, *314*, 964–967; b) S. Yean, L. Cong, C. T. Yavuz, J. T. Mayo, W. W. Yu, A. T. Kan, V. L. Colvin, M. B. Tomson, *J. Mater. Res.* **2005**, *20*, 3255–3264; c) V. Chandra, J. Park, Y. Chun, J. W. Lee, I. C. Hwang, K. S. Kim, *ACS Nano* **2010**, *4*, 3979–3986; d) K. P. Raven, A. Jain, R. H. Loeppert, *Environ. Sci. Technol.* **1998**, *32*, 344–349.

[7] a) G. Morin, Y. Wang, G. Ona-Nguema, F. Juillot, G. Calas, N. Menguy, E. Aubry, J. R. Bargar, G. E. Brown, Jr., *Langmuir.* **2009**, *25*, 9119 – 9128; b) Y. Wang, G. Morin, G. Ona-Nguema, F. Juillot, G. Calas, G. E. Brown, Jr., *Environ. Sci. Technol.* **2011**, *45*, 7258 – 7266.
[8] a) F. Chen, W. B. Bu, Y. Chen, Y. C. Fan, Q. J. He, M. Zhu, X. H. Liu, L. P. Zhou, S. J. Zhang, W. J. Peng, J. L. Shi, *Chem. Asian J.* **2009**, *4*, 1809 – 1816; b) J. Park, K. An, Y. Hwang, J. G. Park, H. J. Noh, J. Y. Kim, J. H. Park, N. M. Hwang, T. Hyeon, *Nat. Mater.* **2004**, *3*, 891 – 895.
[9] T. Zhang, J. Ge, Y. Hu, Y. Yin, *Nano Lett.* **2007**, *7*, 3203 – 3207.
[10] M. M. Shehata, B. Scholten, I. Spahn, H. H. Coenen, S. M. Qaim, *J. Radioanal. Nucl. Chem.* **2011**, *287*, 435 – 442.
[11] a) R. Shi, Y. Jia, C. Wang, *J. Environ. Sci.* **2009**, *21*, 106 – 112; b) A. Violante, M. Pigna, *Soil Sci. Soc. Am. J.* **2002**, *66*, 1788 – 1796.
[12] H. S. Choi, W. Liu, P. Misra, E. Tanaka, J. P. Zimmer, B. I. Ipe, M. G. Bawendi, J. V. Frangioni, *Nat. Biotechnol.* **2007**, *25*, 1165 – 1170.
[13] C. Glaus, R. Rossin, M. J. Welch, G. Bao, *Bioconjugate Chem.* **2010**, *21*, 715 – 722.
[14] A. Luciani, E. Itti, A. Rahmouni, M. Meignan, O. Clement, *Eur. J. Radiol.* **2006**, *58*, 338 – 344.
[15] a) P. Mehlen, A. Puisieux, *Nat. Rev. Cancer* **2006**, *6*, 449 – 458; b) D. X. Nguyen, P. D. Bos, J. Massague, *Nat. Rev. Cancer* **2009**, *9*, 274 – 284.
[16] a) H. Hong, K. Yang, Y. Zhang, J. W. Engle, L. Feng, Y. Yang, T. R. Nayak, S. Goel, J. Bean, C. P. Theuer, T. E. Barnhart, Z. Liu, W. Cai, *ACS Nano* **2012**, *6*, 2361 – 2370; b) H. Hong, Y. Yang, Y. Zhang, J. W. Engle, T. E. Barnhart, R. J. Nickles, B. R. Leigh, W. Cai, *Eur. J. Nucl. Med. Mol. Imaging* **2011**, *38*, 1335 – 1343; c) W. Cai, D. W. Shin, K. Chen, O. Gheysens, Q. Cao, S. X. Wang, S. S. Gambhir, X. Chen, *Nano Lett.* **2006**, *6*, 669 – 676; d) W. Cai, K. Chen, K. A. Mohamedali, Q. Cao, S. S. Gambhir, M. G. Rosenblum, X. Chen, *J. Nucl. Med.* **2006**, *47*, 2048 – 2056; e) D. D. Nolting, M. L. Nickels, N. Guo, W. Pham, *Am. J. Nucl. Med. Mol. Imaging* **2012**, *2*, 273 – 306.
[17] a) J. Xie, K. Chen, J. Huang, S. Lee, J. Wang, J. Gao, X. Li, X. Chen, *Biomaterials* **2010**, *31*, 3016 – 3022; b) J. C. Park, M. K. Yu, G. I. An, S. I. Park, J. Oh, H. J. Kim, J. H. Kim, E. K. Wang, I. H. Hong, Y. S. Ha, T. H. Choi, K. S. Jeong, Y. Chang, M. J. Welch, S. Jon, J. Yoo, *Small* **2010**, *6*, 2863 – 2868; c) R. T. Martin de Rosales, R. Tavare, R. L. Paul, M. Jauregui-Osoro, A. Protti, A. Glaria, G. Varma, I. Szanda, P. J. Blower, *Angew. Chem.* **2011**, *123*, 5623 – 5627; *Angew. Chem. Int. Ed.* **2011**, *50*, 5509 – 5513; d) L. Sandiford, A. Phinikaridou, A. Protti, L. K. Meszaros, X. Cui, Y. Yan, G. Frodsham, P. A. Williamson, N. Gaddum, R. M. Botnar, P. J. Blower, M. A. Green, R. T. de Rosales, *ACS Nano* **2013**, *7*, 500 – 512.

